DTU Library

Quantitative analysis of ultrasound B-mode images of carotid atherosclerotic plaque: correlation with visual classification and histological examination

Wilhjelm, Jens E.; Grønholdt, Marie-Louise; Wiebe, Brit; Jespersen, Søren Kragh; Hansen, Lars Kai; Sillesen, Henrik

Quantitative Analysis of Ultrasound B-Mode Images of Carotid Atherosclerotic Plaque: Correlation with Visual Classification and Histological Examination

J. E. Wilhjelm,* *Member, IEEE*, M.-L. M. Grønholdt, B. Wiebe, S. K. Jespersen, L. K. Hansen, and H. Sillesen

Abstract— This paper presents a quantitative comparison of three types of information available for 52 patients scheduled for carotid endarterectomy: subjective classification of the ultrasound images obtained during scanning before operation, first- and second-order statistical features extracted from regions of the plaque in still ultrasound images from three orthogonal scan planes and finally a histological analysis of the surgically removed plaque. The quantitative comparison was made with the linear model and with separation of the available data into training and test sets. The comparison of subjective classification with features from still ultrasound images revealed an overall agreement of 60% for classification of echogenicity and 70% for classification of structure. Comparison of the histologically determined relative volume of soft materials with features from the still images revealed a correlation coefficient of $r = -0.42 (p = 0.002)$, for mean echogenicity of the plaque region. The best performing feature was of second order and denoted Contrast $(r = -0.5)$. Though significant, the latter correlation is probably not strong enough to be useful for clinical prediction of relative volume of soft materials for individual patients. Reasons for this is discussed in the paper, together with suggestions for improvements.

Index Terms— Carotid plaque, feature extraction from ultrasound images, gray level co-occurrence matrix, quantitative histology.

I. INTRODUCTION

IN most industrialized countries, stroke remains the third most common cause of death and many patients surviving a stroke experience permanent disabilities, often resulting in inability to work or even the need for help to meet daily tasks. Twenty to thirty percent of strokes are believed to be caused by emboli arising from atherosclerotic carotid artery plaques, and recent studies have shown that the risk of stroke is reduced by more than 50% by surgical removal (endarterectomy) of plaques that caused a diameter reduction of more than 70% [9], [30] assessed by angiography. However, not all carotid plaques are necessarily harmful and as carotid endarterectomy carries a considerable risk for the patient, optimized selection of patients for operation is crucial.

So far, ultrasound Doppler examination has become well established for assessment of *the lumen reduction* caused by the carotid plaque [12], [26], [28], and the method has in some institutions supplanted arteriography even when carotid endarterectomy is planned. [16] However, during the last decade an increasing number of reports have indicated that B-mode ultrasound images of the carotid plaque reveal features (echogenicity and structure) related to the presence of brain infarcts on computed tomography images [17] and to the risk of developing new neurological symptoms [2], [6], [20], [22], [25], [32], [38]. In other studies, where carotid endarterectomy was involved, the intensity of the reflected signals has been related directly to the amount of calcification and inversely to the amount of soft materials (lipids and hemorrhage) [8], [13], [31]. In addition, plaques with a heterogeneous appearance on the ultrasound image (i.e., echogenic areas mixed with anechoic areas) contain more calcification compared to homogeneous plaques [8], [18]. With few exceptions, this work has been performed using subjective visual classification of the ultrasound images.

To obtain a more objective approach, El-Barghouty *et al.* [10] calculated the echogenicity associated with carotid plaques and found that those with a low median gray-scale value were associated with cerebral infarctions identified on computed tomography images much more commonly as compared to those with a high median gray-scale value. Later, El-Barghouty *et al.* [11] found a direct correlation between median echogenicity of carotid plaques and content of fibrous tissues and an inverse correlation to content of soft materials.

Quantitative image analysis has previously been applied to echocardiographic images, [7], [39] ultrasound images of the breast [14], [15] and to ultrasound images of liver [4], [24], [29], [36], [40]. In the latter investigations, a large number of features has been calculated from regions located inside liver
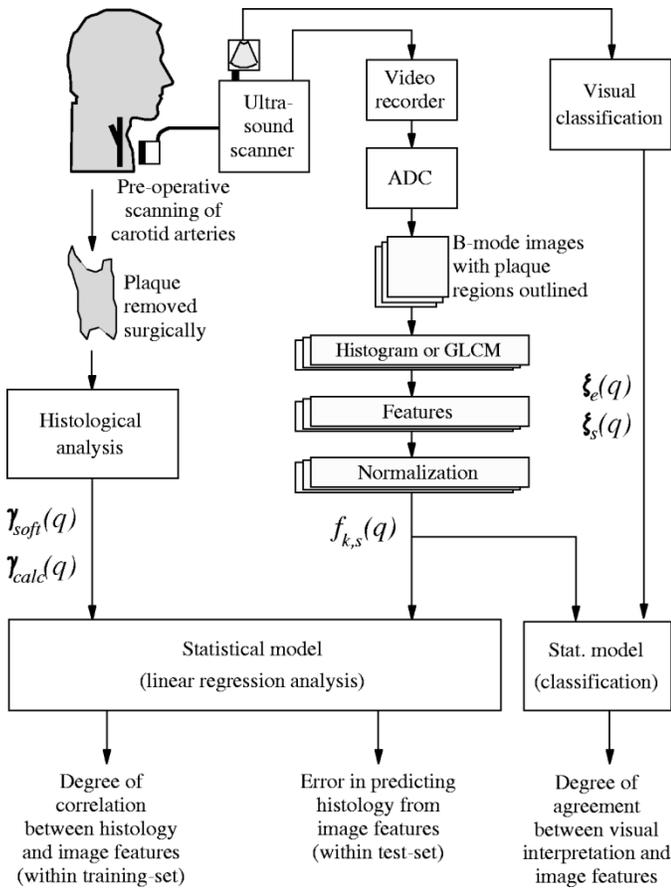
Fig. 1. Overview of data sources and analysis methods.

tissue on B-mode images. By means of different calculation schemes, these features have then been used to classify each organ into a few classes (normal tissue and different classes of diseased tissue). Not all of these investigations involved model design based on a subset of the available data (training set) followed by performance analysis of this model based on the remaining data (test set). When analyzing multiple features, this can be an important tool in reducing—but not eliminating—the risk of finding accidental correlation between a given feature and the available data, since the test error is an unbiased performance measure [3].

In the present study, statistical features were calculated from carotid plaque regions in digitized video ultrasound B-mode images. It was investigated, to which extent these features correlated with subjective visual classification of the plaque appearance, as evaluated by the ultrasonographer during scanning and how well the features correlated to the histological composition of the plaque specimen.

II. MATERIALS AND METHODS

A. Subjects and Clinical Recording Procedure

A schematic outline of the investigation is given in Fig. 1. Fifty-two patients were selected randomly out of 119 consecutive patients that had experienced ipsilateral neurological symptoms. The patients underwent prophylactic carotid en-

darterectomy 2.7 ± 2.8 (mean $\pm$ SD) days after ultrasound examination. All patients gave informed consent and the study protocol was approved by the medical ethics committee for Copenhagen and Frederiksberg counties (#KF 01-375/94).

Preoperatively the stenotic carotid artery was evaluated with high resolution B-mode, color flow mapping (CFM) and spectral Doppler ultrasonography. In each patient, representative scan-sequences were recorded in the lateral, anterior and cross-sectional planes with and without color Doppler on video tape for later analysis. The three planes recorded are denoted $s = 1, 2$, and 3, respectively. Effort was made to ensure that the cross-sectional plane was at the location of maximal stenosis. The atherosclerotic lesion (plaque) in the carotid artery was classified on-line by a single experienced investigator (MLG) using the following characteristics: plaque echogenicity was either *strong* (echogenic), *intermediate*, or *weak* (anechoic) relative to the intima-media complex of the far carotid wall; plaque structure was described as *homogeneous* or *heterogeneous* [8], [37]. Using generally accepted Doppler criteria [26] the degree of stenosis was also estimated. The mean degree of stenosis was 79% (range 50–95%).

Reviewing the videotapes, B-mode images from the three different scan planes of each carotid artery were digitized and stored in a computer for further analysis. Selection was done, such that plaque contour/border, area, and contrast were optimized, subjectively judged. For each image, outline(s) of plaque region(s) were drawn by the same investigator (MLG) who had previously done the ultrasound examination. This investigator was unaware of the results of the histological analysis and the feature extraction. The outline was drawn on the B-mode image under visual support by the corresponding CFM image to best identify the border of the plaque. In cases with acoustic shadow, a possible part of the plaque in the shadow region—which typically would be black—was not included. Fig. 2(a) provides an example of such outlines while Fig. 2(b) shows the corresponding surgically removed plaque.

B. Ultrasound System and Digitalization Equipment

A diagnostic ultrasound scanner (RX 400, Interspec, ATL, Bothell, WA, USA) with a 128-element 5- to 10-MHz linear array transducer was used for the clinical recordings. Transmit focus of the scanner was always set to the depth considered. Image sequences were transferred to a super VHS video recorder (type AG-7350, Panasonic). Still images were later digitized (with $G = 256$ gray levels) with a frame grabber (Targa 2000-E, Truevision Inc., Indianapolis, IN) and captured with image processing software (Image Pro v1.2.01, Media Cybernetics, Silver spring, MD). The vertical and horizontal width of the point-spread function (psf), was estimated with a string phantom and found to be $(\Delta x, \Delta y) = (2\lambda, 2.5\lambda)$ and $(2.5\lambda, 3.5\lambda)$ at a depth of 2 and 3 cm, respectively. One wavelength λ is equal to 0.2 mm (= 2 pixels) at 7.5 MHz assuming the speed of sound to be 1540 m/s.

The image degradation due to the video recorder was investigated by considering a point-like character on the scanner

TABLE I
KEY PARAMETERS IMPORTANT FOR PERFORMANCE OF ESTIMATES OF FIRST- AND SECOND-ORDER FEATURES. THE VALUES
GIVEN AS MEAN ±SD WERE BASED ON 52 PATIENTS. THE p-VALUES ARE THE RESULTS OF COMPARING THE LATERAL
SCAN PLANE TO THE ANTERIOR AND TO THE CROSS-SECTIONAL SCAN PLANES. NS = NOT SIGNIFICANT ($p \geq 0.01$)

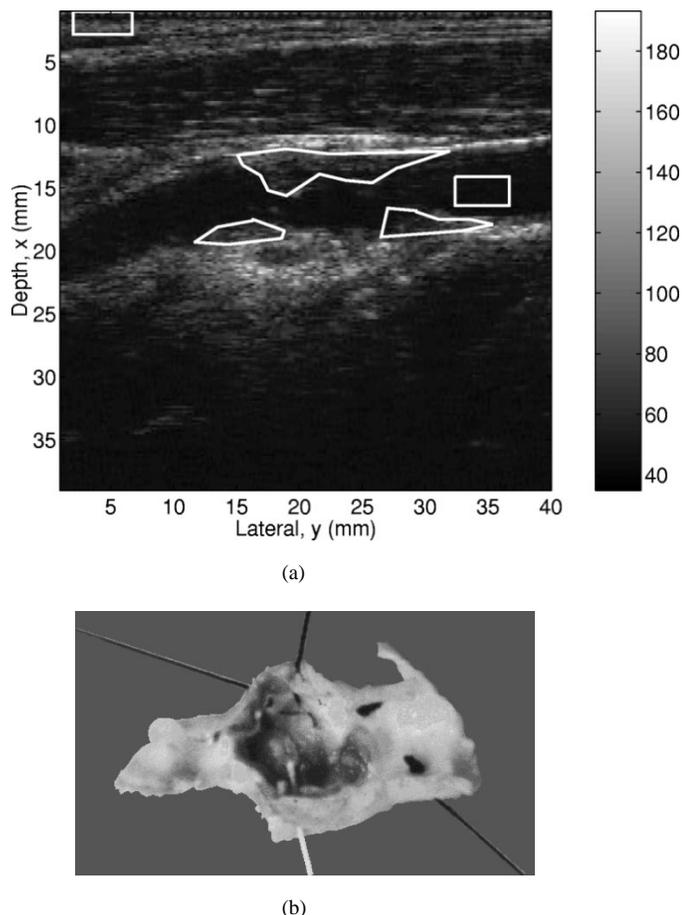| s (scan plane)	Mean depth (pixels)	Area (pixels)	Vertical extent (pixels)	Horiz. extent (pixels)
1 (lateral)	197 ±38	4487 ±2273	20 ±5	54 ±18
2 (anterior)	174 ±46 $p<.00003$	5431 ±3101 NS	22 ±7 NS	70 ±31 $p<.0003$
3 (cross-sectional)	194 ±46 NS	3159 ±1539 NS	29 ±10 $p<7\cdot10^{-8}$	39 ±18 $p<.000002$

(a)

(b)

Fig. 2. (a) Typical B-mode image of an atherosclerotic carotid artery with plaque regions outlined. This particular plaque was characterized as anechoic and homogeneous. The upper left rectangular region was used to study the mean gray level in the muscle tissue (Fig. 3). The rectangular region in the lumen was used for calibration purposes. (b) The formalin fixed plaque specimen after surgical removal. The picture shows the opened plaque from the proximal common carotid artery (right) to the distal internal carotid artery (left). The plaque is approximately aligned with the ultrasound image. The length is 32 mm.

screen. Images digitized directly and after storage on the video recorder were compared, and the video recorder was found to introduce—for a given pixel—a root-mean-square (rms) error on the gray-level value of approximately five gray levels. This was partly due to noise, partly because the output image from the video recorder was lowpass filtered in the horizontal direction. The smearing due to the latter was low, compared to the horizontal extent of the psf.

C. Histological Analysis of Removed Plaque

The carotid plaques were removed during surgery and fixed in 4% formalin. After measuring the length of the entire specimen, transverse blocks of length 2–3 mm were cut. The external carotid was discarded. After processing the blocks in paraffin, microtome slices (of 4 μm thickness) were cut from each block and stained with haematoxylin, eosin and Verhoeff. Histological analysis was performed by an experienced pathologist (BW) using a microscope connected to a computer running an image analysis program. From the microscopic image of each stained slice, the regions of soft materials (lipids, haemorrhage, and thrombus), fibrous tissues and calcification were identified subjectively by the pathologist and the area calculated. By assuming a constant interblock distance, the relative volume of each component, e.g., $\gamma_{\text{calc}}(q)$, was finally calculated. Thus, $\gamma_{\text{soft}}(q) + \gamma_{\text{fibr}}(q) + \gamma_{\text{calc}}(q) = 1$.

D. Scan Plane Statistics

To decide whether all three scan planes should be used in the subsequent analysis, the following parameters were considered for all scan planes: 1) plaque depth, which preferably should be as low as possible to minimize the distortion of the intervening tissue layer between transducer and plaque; 2) plaque area, which preferably should be as large as possible to represent as much plaque as possible; 3) mean plaque extent in the horizontal and vertical image directions, which should be as large as possible to have as many co-occurrences as possible for generation of second-order image features.

The mean values and standard deviations of these parameters are shown in Table I. To investigate if these values were associated with a statistically significant difference between scan planes, p-values were calculated between scan plane 1 and 2 as well as between scan plane 1 and 3. The p-values were calculated with Wilcoxon matched-pairs signed-ranks test. The null hypothesis is that the difference ($d_i = x_i - y_i$) between the members of each pair (x_i, y_i) has median value zero.

The four parameters in Table I characterize the plaque regions in the ultrasound images. If either scan plane two or

three was associated with parameters much worse than scan plane one, it could be expected that this scan plane would add less information to the subsequent image analysis than the other scan planes. Table I indicates that when all four parameters are considered together, neither scan plane two nor three has systematically inferior parameters than scan plane one.

E. Image Calibration

The gain level of the ultrasound scanner was adjusted for each patient so that echoes just began to appear in the blood lumen in the image of the lateral scan plane. This was necessary since the intervening tissue layer and its orientation were different from patient to patient. Nevertheless, inconsistency in overall gray level might be a potential problem as also pointed out by Kadah *et al.* [24]. A possible solution would be to find a region or a characteristic in the B-mode image that can be considered to have a common behavior.

In the present investigation a rectangular box was placed near the plaque in the unaffected lumen of the artery on the ultrasound image, as illustrated in Fig. 2(a). The mean gray level of the blood region is due to scattering from blood in the main lobe, electrical noise and various echoes produced by sidelobes and grating lobes. It was verified that increasing the gain resulted in an approximately linear increase in mean gray level of this box over the range of gains used. Thus, the mean level of the blood region depended on variations in gain setting from patient to patient (e.g., too high adjustment of the gain with a given attenuation of the intervening tissue layer between transducer and plaque). As a simple attempt to improve the consistency in overall gray level between patients, each image was calibrated by subtracting the mean gray level of the blood region from that image and setting possible negative values in the resulting image to zero (it was assumed that any gray level below that of the mean blood level could be considered noise).

F. Feature Extraction from Plaque Regions

The information in the plaque region(s) of each B-mode image was reduced to a number of scalars by means of extraction of first- and second-order texture statistics. As seen in Fig. 2(a), the plaque regions were highly irregular. Each plaque region was referred to as a matrix $I(x, y)$, where a subgroup of all the elements, N, corresponds to "plaque pixels" and the rest were excluded from further analysis. The normalized feature value from a given plaque, q, and a given plane, s, is identified by the symbol $f_{k,s}(q)$, where k is the feature number.

Sixteen first-order gray-level features were calculated from the normalized gray-level histogram. Specifically, if $h(g)$ is the number of image pixels with gray level g, such that $\Sigma_{g=0}^{G-1} h_g = N$, then the normalized histogram, $H(g) = h(g)/N$, is the empirical probability density function for single pixels. An overview of the first-order features is given in the Appendix. When more than one plaque region was identified in the image, $h(g)$ was calculated for each region and then added, and the result normalized, before further analysis.

Seven second-order features were calculated based on the gray-level co-occurrence matrix (GLCM) [5], [29]. This basis for calculating second-order features has previously been used in attempts to classify tissue from ultrasound images [4], [5], [24], [29], [36], [39], [40]. The GLCM is a measure of the co-occurrences in the image and is calculated for a given displacement vector, $\underline{d} = (d, \theta)$. A given cell in the GLCM, $c(i, j)$, indicates how many pairs of two pixels, separated by the displacement vector $\underline{d}$, that have the gray levels i and j, respectively. An overview of the second-order features are given in the Appendix. When a given B-mode image contained more than one plaque region, the GLCM's for the different regions were added to yield one single GLCM per B-mode image. The GLCM is normalized, so that each element is an estimate of empirical probability.

As described above, the GLCM is calculated based on two parameters. The angle was restricted to $0°$ (horizontal direction, left to right in the image) and $90°$ (vertical direction (i.e., along the ultrasound beam), from top to bottom in the image). For each of these angles, the lower bound on the step size is dictated by the extent of the psf, as found in Section II-B. The upper bound is dictated by the desire to obtain a reasonably high number of pairs in the GLCM (see Table I, columns four and five). These considerations lead to the following values for (d, θ): $(7, 0°)$, $(10, 0°)$, $(15, 0°)$, $(20, 0°)$, $(30, 0°)$, $(5, 90°)$, $(8, 90°)$ and $(12, 90°)$. Note that $c(i, j; d, \theta) = c(i, j; d, \theta + 180°)^T$.

In the subsequent analysis, the features obtained from each of the three scan planes were averaged, if not explicitly stated otherwise.

G. Statistical Model for Evaluation of Performance

Features extracted from the plaque regions in the B-mode images were correlated to the visual classification as well as to the histological results using the linear model [23], $\underline{Y} = \underline{\underline{X}} \, \underline{\beta}$.

To facilitate comparisons between the performance of different features, each feature vector was offset and normalized so that it ranged from zero to unity. The histological results, e.g., $\gamma_{\mathrm{calc}}(q)$, were also in the interval zero to unity.

The analysis of correlation between image features and visual classification was done exactly the same way for echogenicity and structure (identified by subscripts e and s, respectively) and, therefore, only echogenicity is considered below. The visual classification of echogenicity—denoted $\zeta_e(q)$ for plaque q—was given in three classes by the independent variable $\underline{\underline{X}}$ and the feature values were specified by the dependent variable, $\underline{Y}_k$, for feature k. Specifically, when the number of classes were L_e, $\underline{\underline{X}}$ would be a matrix of height Q and width L_e, where each row of $\underline{\underline{X}}$ contains zeros, except at the column which is identical to the class where the value was unity

$$X(q, j) = \begin{cases} 1, & \text{for } j = \zeta_e(q) \\ 0, & \text{otherwise.} \end{cases}$$

Likewise, $\underline{Y}_k$ was a column vector of height Q containing the Q values of a given feature k. The estimated regression parameter set, $\underline{\hat{\beta}}_k$, thus became a column vector of height L_e.

$\hat{\underline{\beta}}_k$ represents the least squares solution. When the elements β_1, β_2, and β_e are known ($L_e = 3$), and the class values were positively related to feature values, the three classes would be defined by the intervals $[0; (\beta_1 + \beta_2)/2]$, $](\beta_1 + \beta_2)/2; (\beta_2 + \beta_3)/2]$, and $](\beta_2 + \beta_3)/2; 1]$. $\underline{Y}_k$ could subsequently be used with the class intervals to find the estimated classes. The following equation is used as a measure of how well the estimated class agrees with the visual classification [1]

$$\kappa = \frac{p_0 - p_e}{1 - p_e} \qquad (2)$$

where p_0 and p_e are the relative number of agreements and the relative number of expected agreements by chance, respectively. Therefore, $\kappa \leq 1$. For echogenicity, the following measure was used to quantify mean classification error: $R_{v,e} = E_q\{|\zeta_e(p) - \hat{\zeta}_e(p)|\}$, where $\zeta_e(p)$ and $\hat{\zeta}_e(p)$ are the classes given during ultrasound scanning and estimated from the feature values, respectively. $E_q\{\cdot\}$ denotes mean value over all plaques.

For the analysis of correlation between image features and histological results, column vector $\underline{Y}$ represented the histological results and column vector $\underline{X}$ contained the values of a given feature. In the linear model $\underline{\underline{X}} = [\underline{X}\ \underline{1}]$, where $\underline{1}$ is a column vector with only ones and with the same height as $\underline{X}$. Thus $\underline{\beta}$ holds the regression parameters (*slope* and *y-axis intercept*). The least squares solution, $\hat{\underline{\beta}} = (\underline{\underline{X}}'\underline{\underline{X}})^{-1}\underline{\underline{X}}'\underline{Y}$, is a maximum-likelihood estimate, provided $\underline{Y}$ follows a normal distribution. The residue is: $\underline{\varepsilon} = \underline{Y} - \underline{\underline{X}}\,\hat{\underline{\beta}}$. Provided $\underline{\varepsilon}$ follows a normal distribution, the p-value is found as well [23]. The null hypothesis is that the regression parameter is zero (slope of regression line is zero), or that there is no correlation between $\underline{X}$ and $\underline{Y}$. Finally, a measure of the mean error calculated over all observations (plaques) is: $R_h = E_q\{|\underline{\varepsilon}|\}$. Note that using absolute values instead of squared values, when calculating $R_{v,e}$, $R_{v,s}$ and R_h provides a more robust estimate of the error [35].

All features were tested to evaluate their ability to predict the visual classification and the histological results by applying the following two-step procedure.

1) First and second-order features were calculated for the entire data set ($Q = 52$ plaques) and correlated to both the visual classification and to the histological results. Then features fulfilling a given set of requirements—to be stated in Section III—were extracted.

2) The hypothesis that these "significant" features could be used for prediction was then tested by splitting the data set into a training set (80%) and a test set (20%). The analysis of the training set provided the regression parameters, $\hat{\underline{\beta}}_{\text{train}}$, and the test set could then be used to evaluate the performance. Different training and test sets were extracted $M = 50$ times from the entire data set by means of resampling. It was verified that the results did not change with a larger number of re-samplings of the training and test sets. If $R_{\text{test}}(m)$ takes the value of one of the error measures ($R_{v,e}$, $R_{v,s}$, or R_h) calculated for the plaques in the test set for a given feature at resampling m, then the mean test error for this feature
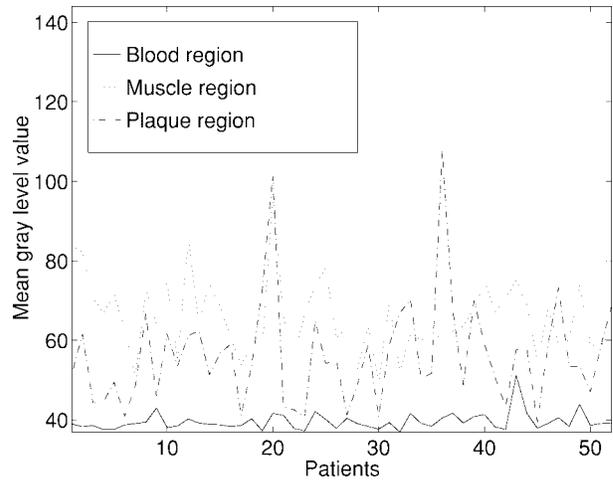

Fig. 3.   The variation of mean gray level (uncalibrated) in the lateral scan plane ($s = 1$) for the three types of regions outlined in Fig. 2. The data points are connected together only to ease interpretation.

is calculated as

$$\overline{R}_{\text{test}} = \frac{1}{M} \sum_{m=1}^{M} R_{\text{test}}(m). \qquad (3)$$

A measure similar to (3) is defined for the training set.

III. RESULTS

A. Mean Gray-Level Variation over Patients

The mean gray level inside the blood, muscle and plaque regions shown in Fig. 2 is plotted in Fig. 3. The mean gray level of the blood region only showed minor fluctuation (with a few distinct outliers), when compared to the mean gray level in the muscle region and plaque regions. For all three scan planes, the mean gray level of the blood region was 40 ± 2.

B. Correlation Between Visual Classification and Image Features

Table II lists the features where the mean classification error evaluated for all patients were below $R_{v,e} = 0.42$ and $R_{v,s} = 0.26$ for echogenicity (three classes) and structure (two classes), respectively. Examples of the classification frequencies within the training and test sets for echogenicity and plaque structure are provided in Figs. 4 and 5, respectively.

In both cases it is seen that performance within the training set is quite close to performance within the test set. For classification of echogenicity, the test set revealed that $\kappa_{\text{test}} = 0.4$ and the agreement was 60%. For classification of structure, the test set revealed that $\kappa_{\text{test}} = 0.41$ and agreement was 70%. A κ in the interval [0.21; 0.40] and [0.41; 0.60] is normally associated with fair and moderate strength of agreement, respectively [1].

It should be expected that the more data there is available, the better the prediction performance will be. Therefore, the feature used to produce Fig. 4 was studied in more detail. Specifically, in Fig. 6, the mean classification error is plotted as a function of different combinations of scan planes. It is seen, that—on average—the error decreases with increasing number of scan planes.

TABLE II
OVERVIEW OF FEATURES FOR CLASSIFICATION OF ECHOGENICITY AND STRUCTURE, WHEN THE MEAN
CLASSIFICATION ERROR OVER ALL 52 PLAQUES WERE BELOW $R_{v,e} = 0.42$ AND $R_{v,s} = 0.26$, RESPECTIVELY

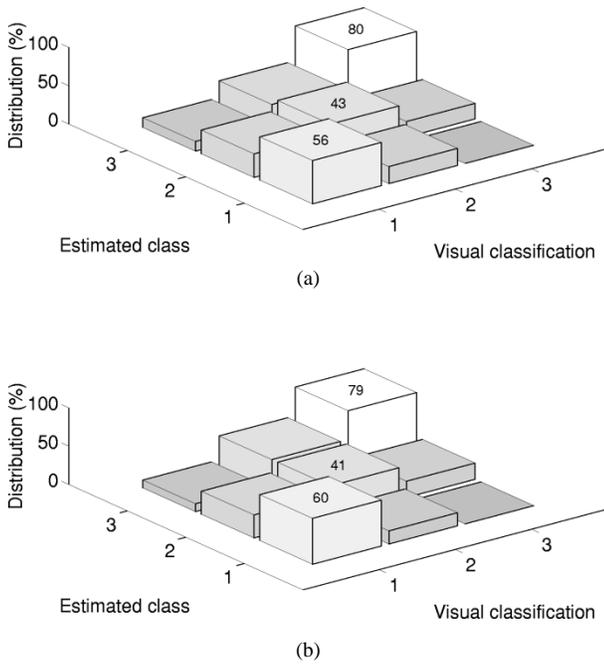| Type	Name	Type	$\overline{R}_{train}$	$\overline{R}_{test}$
Echogenicity	Median (f_3)	First order	0.43	0.42
	10 %ile (f_{11})	First order	0.40	0.43
	25 %ile (f_{12})	First order	0.40	0.42
	50 %ile (f_{13})	First order	0.41	0.42
Structure	Median (f_3)	First order	0.26	0.28
	50 %ile (f_{13})	First order	0.26	0.30
	Contrast (15, 0°) (f_{22})	Second order	0.26	0.33
	Correlation (30, 0°) (f_{20})	Second order	0.27	0.23
	Contrast (30, 0°) (f_{22})	Second order	0.26	0.34

Fig. 4. (a) Classification frequencies (training set) for echogenicity class estimated from image feature Median (f_3) and echogenicity class found by visual inspection. 1 = echogenic, 2 = intermediate and 3 = anechoic. (b) Performance of the feature as revealed by the test set.

Fig. 5. (a) Classification frequencies (training set) for structure class estimated from image feature Contrast (15, 0°) (f_{22}), and structure class found by visual inspection. 1 = homogeneous and 2 = heterogeneous. (b) Performance of the method as revealed by the test set.

C. Agreement Between Image Features and Histology

1) Plaque Contents Statistics: The mean and standard deviation of the histological results are given in Table III. Compared to fibrous tissues, calcified materials exhibit increasing echogenicity and increasing dependence on insonification angle [34]. They are, therefore, potentially distinguishable from each other, but because the relative volume of fibrous tissues for a given plaque is $\gamma_{\text{fibr}}(q) \cong 1 - \gamma_{\text{soft}}(q)$, only $\gamma_{\text{calc}}(q)$ will be considered in addition to $\gamma_{\text{soft}}(q)$. There was no statistical significant correlation between $\gamma_{\text{calc}}(q)$ and $\gamma_{\text{soft}}(q)$ or $\gamma_{\text{fibr}}(q)$.

2) Correlation Between Soft Materials Content and Mean Echogenicity: As the main constituents of the plaque were soft materials and fibrous tissues, and these have different backscattering characteristics, the analysis is commenced

by a comparison between relative volumetric content of soft materials and mean echogenicity of the plaque regions. The result, when all three scan planes were considered together, is shown in Fig. 7, while Table IV lists p-values and correlation coefficients, when the planes were considered individually and combined.

3) Overall Correlation Between Image Features and Histology: When testing all features, a feature was considered significant if it fulfilled the condition: $p < 0.001$ and $R_h < 0.15$ (with this low p-value, only a few of the "best" features were extracted). Based on this, significant features were found for estimation of $\hat{\gamma}_{\text{soft}}(q)$ (with and without calcified plaques removed from the analysis), but not for estimation of $\hat{\gamma}_{\text{calc}}(q)$. The features are identified in Table V. Notice the small difference obtained when calcified plaques are removed. The result for the feature associated with the smallest mean test error is

Fig. 6. Mean classification error when using feature Median (f_3) for prediction of echogenicity class when each individual scan plane and combinations hereof were used.

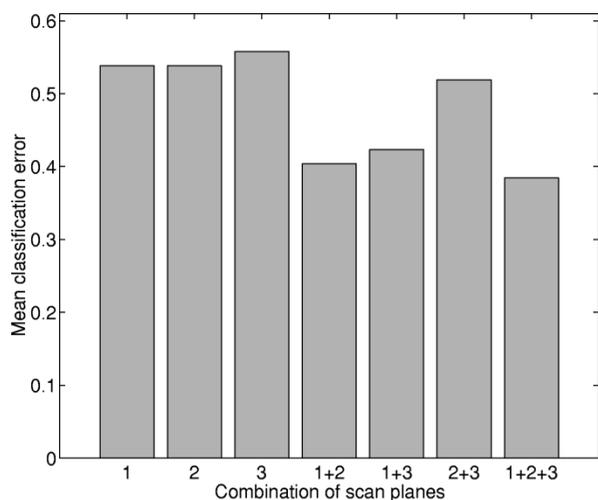### TABLE III
THE RELATIVE VOLUME OF PLAQUE MATERIALS IN THE 52 PLAQUES ANALYZED HISTOLOGICALLY

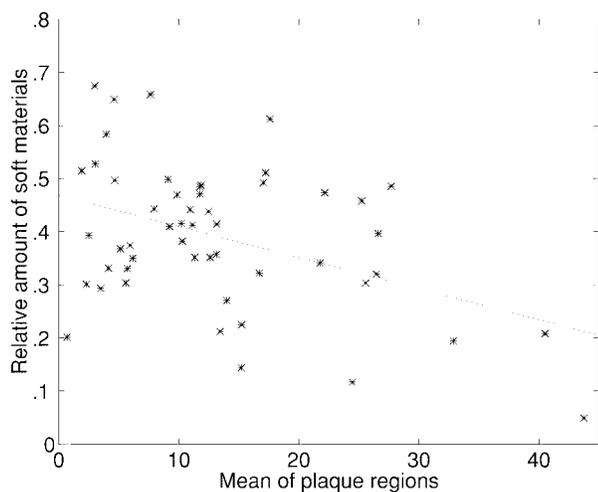| $E_q\{\gamma_{\text{soft}}\}\pm\text{SD}_q\gamma_{\text{soft}}$	$E_q\{\gamma_{\text{fibr}}\}\pm\text{SD}_q\gamma_{\text{fibr}}$	$E_q\{\gamma_{\text{calc}}\}\pm\text{SD}_q\gamma_{\text{calc}}$
$39.5 \pm 13.6\%$	$59.3 \pm 13.8\%$	$1.3 \pm 1.5\%$

Fig. 7. Relative volumetric content of soft materials plotted against (unnormalized) Mean gray level (f_4) of the plaque regions in all three planes. The correlation coefficient is: -0.42. The regression line shows the least-squares error fit. Note that the mean gray level has been adjusted as described in Section II-V.

TABLE IV
p-VALUES AND CORRELATION COEFFICIENTS FOR THE CORRELATION BETWEEN RELATIVE VOLUMETRIC CONTENT OF SOFT MATERIALS AND THE MEAN GRAY LEVEL (f_4) EXTRACTED FROM INDIVIDUAL SCAN PLANES AND THE AVERAGE OF ALL THREE SCAN PLANES

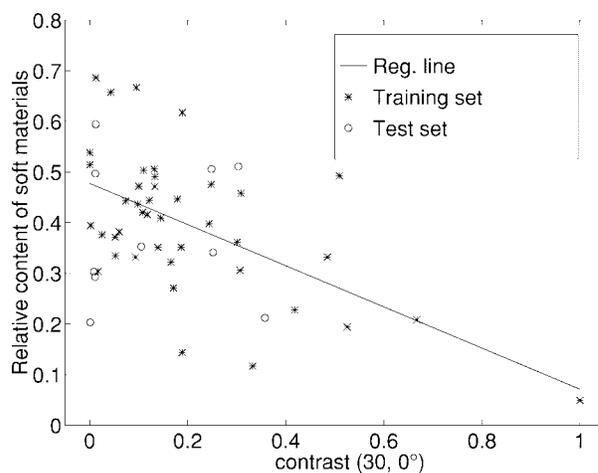| Plane	p	r
1	0.0004	-0.47
2	0.4	-0.12
3	0.0005	-0.47
1+2+3	0.002	-0.42

Fig. 8. Result of a specific training and test set for feature Contrast (30, $0°$) (f_{22}) used for predicting of soft materials. When the entire data set was analyzed (52 plaques), the correlation coefficient became $r =- 0.50$. When the right most data point was removed from the set (i.e., the one with a feature value of unity), the correlation coefficient became $r =- 0.38$.

shown in Fig. 8. No Bonferroni correction was applied to the p-values of Table V, thus, the p-values can only be used for ranking the features.

IV. DISCUSSION

A. Correlation Between Image Features and Visual Classification

These results featured the best correlation, however, a number of reasons could be responsible for the fact that the agreement was not higher. The visually estimated class gives an overall impression of the appearance of the entire plaque when imaged in real time with at least three different scan planes. The class estimated by feature extraction was based on only three still images per patient. Although intended to, these may not be fully representative of the entire plaque. On the other hand, it is clear from Fig. 6, that the more planes that were used in the analysis, the smaller the classification error.

For classification of echogenicity, the agreement is only fair. One of the reasons for that is the definition of classes: plaques that created an acoustic shadow were mainly classified by the ultrasonographer as echogenic. However, such a plaque is not necessarily (uniformly) echogenic. Taken into consideration that 27% of the plaques had shadows, this could be one of the main explanations. Careful investigation of the mean gray level of the plaques that were classified as echogenic showed a bimodal histogram.

The features listed in Table II can be physically related to the characteristics that were to be predicted: echogenicity is closely related to the Median gray level (f_3) of the regions and to Percentiles ($f_{11} - f_{13}$) of the histograms of the regions. With respect to structure, the two first-order-features are the same as for echogenicity, and one explanation for this unexpected result is that the more heterogeneous the plaque region appears, the higher the overall gray level (analyzing the relation between the two groups showed that while most anechoic

TABLE V

OVERVIEW OF FEATURES FOR PREDICTION OF RELATIVE VOLUME OF SOFT MATERIALS AND RELATIVE VOLUME OF SOFT MATERIALS WHEN CALCIFIED PLAQUES WERE REMOVED FROM THE ANALYSIS. THE p-VALUES WERE CALCULATED FOR THE TRAINING SET AS THE AVERAGE OF THE 50 RESAMPLINGS. THE REGRESSION PARAMETERS WERE IN THE FOLLOWING RANGES: $0.432 < \alpha < 0.473$ AND $-0.37 < \beta < -0.272$. α AND β ARE THE y-AXIS INTERSECTION AND THE SLOPE OF THE REGRESSION LINE, RESPECTIVELY

Type	Feature name	$\overline{p}$	$\overline{R}_{train}$	$\overline{R}_{test}$
Soft materials (52 plaques)	10 %ile (f_{11})	0.0006	0.097 ±0.006	0.11 ±0.024
	25 %ile (f_{12})	0.0009	0.099 ±0.006	0.11 ±0.024
	Contrast (20, 0°) (f_{22})	0.0005	0.097 ±0.006	0.10 ±0.024
	Contrast (30, 0°) (f_{22})	0.0002	0.095 ±0.006	0.10 ±0.023
	Contrast (5, 90°) (f_{22})	0.0002	0.096 ±0.006	0.10 ±0.024
Soft materials, but with calcified plaques removed from the analysis (47 plaques)	10 %ile (f_{11})	0.0010	0.10 ±0.006	0.11 ±0.024
	Contrast (20, 0°) (f_{22})	0.0008	0.10 ±0.006	0.11 ±0.027
	Contrast (30, 0°) (f_{22})	0.0003	0.10 ±0.006	0.10 ±0.027
	Contrast (5, 90°) (f_{22})	0.0004	0.10 ±0.006	0.11 ±0.025

plaques were classified by the operator as homogeneous, many echogenic plaques were classified as heterogeneous). On the other hand, the three second-order features are all measures of the degree of homogeneity of the image [e.g., the more heterogeneous the lower the value of Correlation (f_{20})]. Note, though, that especially for prediction of the structure, the best performing feature will depend on the human observer's perception of homogeneous and heterogeneous structures.

In a similar study [27], 47 high-quality images were recorded from ten patients and analyzed with four first-order and two second-order features. Only Mean gray level (f_4) and Entropy (f_{18}) distinguished between the classes in echogenicity and structure, respectively. In our study, Mean gray level (f_4) performed well with respect to echogenicity while Entropy (f_{18}) did not appear well suited with respect to structure. One of the major differences in methodology was that the visual classification apparently was done from the still images in their study (as compared to visual classification during examination in our study), which might in part explain their better results.

B. Correlation Between Image Features and Histology

When using all the plaques for prediction of soft materials, statistically significant correlation was found for a few features, but the training and test errors were much too high for the method to be used in prediction of relative volumetric content in individual plaques.

$\gamma_{\text{soft}}(q)$ approximately followed a normal distribution, so that the linear regression provided a maximum likelihood estimate. Unfortunately, the variation in the signal, $\gamma_{\text{soft}}(q)$, that was to be predicted—as revealed by the standard deviations in Table III—was close to the test error as revealed from Table V.

When the number of scan planes was varied, as done in Table IV, the picture was not as clear as in Fig. 6. This suggests that the results are less reliable compared to those for visual classification. The same tendency was found for the investigation in Section III-C3 (details not presented).

The features in Table V for overall correlation have a straight-forward physical interpretation: The higher the rel-

ative volume of soft materials, the lower the echogenicity, the Percentiles ($f_{11} - f_{13}$) and the Contrast (f_{22}). Table V also reveals that the performance does not get better when plaques with a high relative volume of calcification were removed. This was unexpected, and is another indication that the content of information in the ultrasound images at present appears insufficient for prediction of relative material volume.

The training and test set method was introduced to try to avoid fitting the data when analyzing a large number of features and to be immune to a situation where a few data points have main influence on the results. It is seen that the performances of the training and test sets are very close, indicating that the size of the data set is large enough to provide stable estimates for the given model.

Another study [11] has reported on correlation between content of soft materials and mean gray level in the plaque regions. A comparison between this study and the present is given in Table VI. Both studies yielded a statistical significant correlation. When furthermore comparing the scatter plot in Fig. 7 with the corresponding plot in their work, it can be observed that the correlation was comparable.

C. Limiting Factors

An overview of the most important limiting factors is provided in Table VII, and elaborated on below.

1) Pulse-echo ultrasound is limited by geometrical effects and diffraction effects: A given plaque element will yield different echo signals depending on its *location* and *orientation* relative to the transducer. This variation can be dramatic for fibrous tissues and especially calcified tissues [34]. As the orientation is unknown for the 3D plaques studied here [e.g., Fig. 2(b)], this effect is likely to introduce a large unknown modulation of the echo signal, which will behave as noise in the analysis presented here. A possible method that can reduce the angle-dependence is spatial compound imaging [21]. Finally, the echo signal is changed by the intervening tissue layer between transducer and plaque and this

TABLE VI
COMPARISON OF OUR STUDY TO ANOTHER STUDY, WITH RESPECT TO CORRELATION
BETWEEN MEAN GRAY LEVEL VALUE AND RELATIVE VOLUME OF SOFT MATERIALS

Item	El-Barghouty et al. [11]	This study
Transducer frequency	7.5 MHz	7.5 MHz
Number of patients	52	52
Number of planes	2	3
Transfer via	photographic paper	video recorder
Spearman's correlation coefficient	−0.35	−0.28

TABLE VII
OVERVIEW OF THE MOST IMPORTANT FACTORS LIMITING THE PERFORMANCE OF THE METHODS USED. ALSO GIVEN ARE POSSIBLE STRATEGIES FOR
IMPROVING PERFORMANCE. THE LIST IS ATTEMPTED GIVEN IN DECREASING ORDER OF IMPORTANCE WITHIN THE GROUPS

Category	Item	Description	Possible solution
Ultrasound	1	Geometrical effects, diffraction effects and intervening tissue layer	Spatial compound imaging
	2	Inter-patient variation of backscattered energy due to intervening tissue layer	Calibration with blood
	3	Low SNR from anechoic regions. False low echogenicity due to shadowing effects	Better contrast
Method /technology	4	Still image from only three scan planes	Real-time 3D imaging
	5	Distortion introduced by system components	Use raw echo signal
	6	Uncertainty in location of outline of plaque	Spatial compound imaging
Histological examination	7	Low spatial sampling rate and human interpretation	Computerized interpretation
	8	Difficulties in separating areas of different plaque materials	Classification with neural network
Image analysis	9	Limitations with second-order features. Better selection of parameters for GLCM calculation	Relate region orientation to GLCM parameters

change is spatially varying. All these effects are likely to give low performance in reproducibility studies for the same patient.

2) The intervening tissue layer in the ultrasound path will be different from patient to patient and thus the absolute level of backscattered energy from the plaque will feature an inter-patient variation. The approach used in the present study to compensate for this variation has a number of drawbacks of which the most important could be the contribution of signals from sidelobes and grating lobes to the mean gray level of the rectangular "blood" region in the image. The most obvious solution to this problem is to apply stationary echo-cancelling to the raw signal from blood [33]. To assess the impact of the present calibration technique on the results of this study, it was found that removing the calibration only yielded slightly poorer performance. To further address the problem of different overall gray-level values, the value of each feature due to a linear operation on the original image is tabulated in the Appendix. It can be observed, that except for Correlation (f_{20}), all the features identified as significant in this study are

susceptible to a linear transformation of the original image.

3) For anechoic regions in the plaque, the echo signal might be dominated by noise or echoes from the sidelobes and grating lobes of the ultrasound transducer. Furthermore, acoustic shadowing (e.g., cause by calcification) may cause part of the plaque to be "invisible" and, therefore, not included in the outline.

4) The ultrasonic information was only obtained from three perpendicular planes through the plaque and not the entire 3D plaque structure which is analyzed histologically. The associated error depends on the degree of spatial variation in materials inside the plaque.

5) There are several levels of information loss in the signal processing: The received echo signal is amplified, digitized, envelope detected and logarithmically compressed. These data are then used in a scan conversion algorithm to calculate the gray-level image which is finally "optimized" to provide the most "pleasant-looking" image on the screen. The image is next converted to an *analog* video signal. In this study, the image is furthermore stored on a video recorder before it is digitized

TABLE VIII
OVERVIEW OF FIRST-ORDER FEATURES

Name	Definition	Value after linear operation on original image
Minimal gray level	$f_1 = \min\{I(x,y)\}$	$f_1' = af_1 + b$
Maximal gray level	$f_2 = \max\{I(x,y)\}$	$f_2' = af_2 + b$
Median gray level	f_3 such that $\sum_{g=0}^{f_3} H(g) = 0.5$	$f_3' \sim af_3 + b$
Mean gray level	$f_4 = \sum_g gH(g)$	$f_4' \sim af_4 + b$
Standard deviation of gray levels	$f_5 = \sqrt{\sum_g (g - f_4)^2 H(g)}$	$f_5' \sim af_5$
Coefficient of variation	$f_6 = \frac{f_5}{f_4}$	$f_6' \sim \frac{a}{a + b/f_4} f_6$
Gray level skewness	$f_7 = \frac{1}{f_5^3} \sum_g (g - f_4)^3 H(g)$	$f_7' \sim f_7$
Gray level kurtosis	$f_8 = \frac{1}{f_5^4} \sum_g (g - f_4)^4 H(g) - 3$	$f_8' \sim f_8$
Gray level energy	$f_9 = \sum_g H(g)^2$	$f_9' \sim f_9$
Gray level entropy †	$f_{10} = -\sum_g H(g)\ln(H(g))$	$f_{10}' \sim f_{10}$
Percentiles	f_n such that $\sum_{g=0}^{f_n} H(g) = c$	$f_n' \sim af_n + b$
(10, 25, 50, 75, 90)	$(n,c) = (11, 0.1), (12, 0.25), (13, 0.5), (14, 0.75), (15, 0.9)$	
Histogram width	$f_{16} = P_{15} - P_{11}$	$f_{16}' \sim af_{16}$

†Ignoring values, when $H(g) = 0$.

(again) by a frame grabber. The noise due to the video recorder is believed to play a minor—but not negligible—role, because the rms error was about five gray levels compared to the mean (over patients) of the Standard deviation (f_5) of the gray level of the pixels of the plaque region(s) which was ~12 and because feature calculation involved integration over the entire plaque region.

6) There could be an uncertainty in location of outline of plaque region(s), because it can be very difficult to distinguish between plaque and other structures such as healthy arterial wall or blood. For instance, if blood was included, then the apparent amount of anechoic material would increase. CFM was used as a guidance in placing the outline, but the colored area in a CFM image—especially for regions of slow flow—is very susceptible to scanner setting (gain and highpass filter cutoff). A reproducibility study [19] has been made on a larger set of images, from the lateral scan plane only. Specifically, the outlines on 58 lateral images were redrawn about 3–6 mo. later by the same investigator. The mean bias between the two independent determinations of gray scale median values was −0.4. The coefficient of variation for this measure was 5.5%. This suggests that the outline location is fairly reproducible, even though gray scale median probably is the feature least sensitive to the exact location of outline.

7) The histological analysis, which is used as a "golden standard," has limitations as well: The plaque is "only" sampled (cross-sectionally) every 2–3 mm and the results are interpreted subjectively by a human observer. A reproducibility study [19] was made for the histological analysis as well. The mean bias for a repeated analysis by the same pathologist of ten plaques were 0.6% and 1.1% for lipid and fibrous tissues, respectively. The corresponding coefficients of variations for these measures were 3.5% and 2.2%, respectively.

8) One of the problems with the subjective human interpretation is that histological separation between area of e.g., calcification and lipid may be difficult since calcification may be present within a region with lipid. Also, the tissue class, "fibrous tissues" may have smaller or larger amounts of soft material components interpositioned between the fibers without this showing up in the histological results.

TABLE IX
OVERVIEW OF SECOND-ORDER FEATURES BASED ON THE GLCM WITH G^2 GRAY LEVEL CHANGES. $F_{17} - F_{23}$ ARE IMPLICIT FUNCTIONS OF (d, θ)

Name	Equation	Value after linear operation on original image
Energy	$f_{17} = \sum \sum C(i,j)^2$	$f_{17}' \sim f_{17}$
Entropy†	$f_{18} = -\sum \sum C(i,j) \ln(C(i,j))$	$f_{18}' \sim f_{18}$
Maximum probability	$f_{19} = \max(C(i,j))$	$f_{19}' \sim f_{19}$
Correlation	$f_{20} = \sum \sum \frac{(i-\mu_J)(j-\mu_I)C(i,j)}{\sigma_J \sigma_I}$	$f_{20}' \sim f_{20}$
Diagonal moment	$f_{21} = \sum \sum |i-j|(i+j-\mu_J-\mu_I)C(i,j)$	$f_{21}' \sim a^2 f_{21}$
Contrast	$f_{22} = \sum \sum (i-j)^2 C(i,j)$	$f_{22}' \sim a^2 f_{22}$
Local homogeneity	$f_{23} = \sum \sum \frac{C(i,j)}{1+(i-j)^2}$	-‡

†Ignoring all elements, where $c(i,j) = 0$.   ‡No simple relationship exist.

9) One of the problems with the second-order features is the relatively small plaque region size and the corresponding low count in the GLCM. Specifically, in this study, the values of the pixels in the plaque regions for the 52 plaques in the lateral scan plane occupied a gray-level interval of length approximately 42 ± 22. Thus, only a small region of about 40×40 cells in the GLCM contains information. As the approximate number of occurrences has been found to be 3500 (total mean count in the GLCM for the different step sizes and angles used), each cell in the 40×40 region will contain, on average, approximately two occurrences. Another potential problem is that when the step size in the lateral direction is too large, the calculation is further degraded due to lateral variations in the attenuation of the intervening tissue layer. Eventually, it is possible that better performance could be obtained by selecting the parameters for the second-order features according to orientation and location (depth) of the plaque.

In conclusion, the combined effect of the large number of uncontrolled factors that may influence the gray level of the plaque regions in clinical B-mode images, the corresponding large inter-patient variation and the uncertainty in the histological analysis, seem to explain the only moderate agreement between image features and plaque constituents.

V. CONCLUSIONS

It has been shown that plaque appearance (echogenicity and structure)—as revealed by the ultrasonographer during scanning—can be predicted from still ultrasound images with a reasonable degree of accuracy. This result is especially important in multi-center studies, where interobserver and intraobserver variations make comparisons difficult.

The attempt to predict relative plaque material volume from the still images showed statistically significant results, yet the results were associated with training and test errors comparable to the variation in material content from plaque to plaque. Ignoring possible inaccuracies in the histological analysis, this indicates that the present ultrasound imaging technology is clinically inapplicable for use in prediction of soft and calcified relative plaque volume in individual patients. The main reasons are likely to be related to both the limitations of B-mode ultrasound imaging (geometrical effects, diffraction, etc.) and to the method (too few scan planes, lack of access to raw ultrasound data, etc.). Future methods based on ultrasound imaging for prediction of plaque materials should try to improve on as many of these factors as possible.

APPENDIX
FIRST- AND SECOND-ORDER FEATURES

In this Appendix, all summations runs from zero to $G - 1$, unless otherwise noted. The first-order features are tabulated in Table VIII. They were either calculated directly from the image region, $I(x,y)$, or from the normalized gray-level histogram, $H(g)$ of $I(x,y)$. $I(x,y)$ contains G gray levels from zero to $G - 1$. The third column of Table VIII contains the value of the feature after a linear gray-level transformation of the original image

$$I'(x,y) = aI(x,y) + b \tag{A1}$$

where a and b are constants and $a > 0$. It is assumed that $I'(x,y)$ have values in the interval $[0; G-1]$ so that truncation does not occur. The new histogram becomes $H'(g) = H((g-b)/a)$.

The second-order features [5], [29] given in Table IX are based on the normalized co-occurrence matrix, $C(i,j)$, so that $\sum \sum C(i,j) = 1$. The expressions in Table IX use the following sums of rows and columns in the GLCM: $C_J(i) = \sum_j C(i,j)$ and $C_I(j) = \sum_i C(i,j)$ together with the following mean

values and standard deviations

$$\mu_J = \Sigma \, iC_J(i) \quad \mu_I = \Sigma \, jC_I(j) \tag{A2}$$

$$\sigma_J = \sqrt{\Sigma (i - \mu_J)^2 C_J(i)}$$

$$\sigma_I = \sqrt{\Sigma (j - \mu_I)^2 C_I(j)}. \tag{A3}$$

The linear operation in (A1) on the original image gives the following value of the GLCM: $C'(i,j) = C((i-b)/a, \, (j-b)/a)$ and these row and column sums: $C'_J(i) = C_J((i-b)/a)$ and $C'_I(j) = C_I(j-b)/a)$. The mean and standard deviations becomes: $\mu' = a\mu + b$ and $\sigma' = a\sigma$.

Note that some of the equations presented in the last columns of Tables VIII and IX are still approximate, however, because the discretization involved with calculation of the histograms and the GLCM's introduces a small nonlinear effect.

REFERENCES

[1] D. G. Altman, *Practical Statistics for Medical Research.*, 1st. ed. London, U.K.: Chapman & Hall, 1996.

[2] G. Belcaro, G. Laurora, M. R. Cesarone, M. T. De Sanctis, L. Incandela, E. Fascetti, G. Geroulakos, G. Ramaswami, A. Pierangeli, and A. N. Nicolaides, "Ultrasonic classification of carotid plaques causing less than 60% stenosis according to ultrasound morphology and events," *J. Cardiovasc. Surg.*, vol. 34, pp. 287–94, 1993.

[3] C. Bishop, *Neural Networks for Pattern Recognition.* Oxford, UK: Oxford Univ. Press, 1995.

[4] J. S. Bleck, U. Ranft, M. Gebel, H. Hecker, M. Westhoff-Bleck, C. Thiesemann, S. Wagner, and M. Manns, "Random field models in the textural analysis of ultrasonic images of the liver," *IEEE Trans. Med. Imag.*, vol. 15, pp. 796–801, Dec. 1996.

[5] J. M. Carstensen, "Description and simulation of visual texture," Ph.D. dissertation no. 59. Department of Mathematical Modeling, Technical Univ., Lyngby, Denmark, 1992.

[6] E. M. Cave, N. D. Pugh, R. J. Wilson, G. R. J. Sissons, and J. P. Woodcock, "Carotid artery duplex scanning: Does plaque echogenicity correlate with patient symptoms?," *Eur. J. Vasc. Endovasc. Surg.*, vol. 10, pp. 77–81, 1995.

[7] S. M. Collins, D. J. Skorton, N. V. Prasad, B. O. Olshansky, and J. A. Bean, "Image texture in two dimensional echocardiography," *Comput. Cardiol.*, 1983, pp. 113–116.

[8] "European carotid plaque study group (ECPSG): Carotid artery plaque composition—Relationship to clinical presentation and ultrasound B-mode imaging," *Eur. J. Vasc. Endovasc. Surg.*, vol. 10, pp. 23–30, 1995.

[9] "European carotid surgery trialist' collaborative group (ECST). MRC European carotid surgery trial: Interim results of symptomatic patients with severe (70-99%) or with mild (0-29%) carotid stenosis," *Lancet*, vol. 337, pp. 1235–1243, 1991.

[10] N. El-Barghouty, G. Geroulakos, A. Nicolaides, A. Androulakis, and V. Bahal, "Computer-assisted carotid plaque characterization," *Eur. J. Vasc. Endovasc. Surg.*, vol. 9, pp. 389–393, 1995.

[11] N. M. El-Barghouty, T. Levine, S. Ladva, A. Flanagan, and A. Nicolaides, "Histological verification of computerized carotid plaque characterization," *Eur. J. Vasc. Endovasc. Surg.*, vol. 11, pp. 414–416, 1996.

[12] W. E. Faught, M. A. Mattos, P. S. van Bemmelen, K. J. Hodgson, L. D. Barkmeier, D. E. Ramsey, and D. S. Sumner, "Color-flow duplex scanning of carotid arteries: New velocity criteria based on receiver operator characteristic analysis for threshold stenoses used in the symptomatic and asymptomatic carotid trials," *J. Vasc. Surg.*, vol. 19, no. 5, pp. 818–828, 1994.

[13] T. M. Feeley, E. J. Leen, M.-P. Colgan, D. J. Moore, DO'B. Hourihane, and G. D. Shanik, "Histologic characteristics of carotid artery plaque," *J. Vasc. Surg.*, vol. 13, no. 5, pp. 719–724, 1991.

[14] S. Finette, A. Bleier, and W. Swindell, "Breast tissue classification using diagnostic ultrasound and pattern recognition techniques: I. Methods of pattern recognition," *Ultrason. Imag.*, vol. 5, pp. 55–70, 1983.

[15] S. Finette, A. R. Bleier, W. Swindell, and K. Haber, "Breast tissue classification using diagnostic ultrasound and pattern recognition techniques—II: Experimental results," *Ultrason. Imag.*, vol. 5, pp. 71–86, 1983.

[16] L. J. Fontenelle, S. C. Simper, and T. L. Hanson, "Carotid duplex scanning: Preferred modality for selecting patients for endarterectomy," *J. Vasc. Technol.*, vol. 18, no. 6, pp. 345–349, 1994.

[17] G. Geroulakos, J. Domjan, A. Nicolaides, J. Stevens, N. Labropoulos, G. Ramaswami, G. Belcaro, and A. Mansfield, "Ultrasonic carotid artery plaque structure and the risk of cerebral infarction on computed tomography," *J. Vasc. Surg.*, vol. 20, no. 2, pp. 263–266, 1994.

[18] M.-L. M. Grønholdt, B. M. Wiebe, H. Laursen, T. G. Nielsen, T. V. Schroeder, and H. Sillesen, "Lipid-rich carotid artery plaques appear echolucent on ultrasound B-mode images and may be associated with intraplaque haemorrhage," *Eur. J. Vasc. Endovasc. Surg.*, vol. 14, pp. 439–445, 1997.

[19] M. L. M. Grønholdt, B. G. Nordestgaard, B. M. Wiebe, J. E. Wilhjelm & H. Sillesen, "Echolucency of computerized ultrasound images of carotid atherosclerotic plaques are associated with increased levels of triglyceride-rich lipoproteins as well as increased plaque lipid content," *Circ.*, vol. 97, pp. 34–40, 1998.

[20] A. Iannuzzi, T. Wilcosky, M. Mercuri, P. Rubba, F. A. Bryan, and M. G. Bond, "Ultrasonographic correlates of carotid atherosclerosis in transient ischemic attack and stroke," *Stroke*, vol. 26, no. 4, pp. 614–619, 1995.

[21] S. K. Jespersen, J. E. Wilhjelm, and H. Sillesen, "Multi-angle compound imaging," *Ultrason. Imag.*, vol. 20, pp. 81–102, 1998.

[22] J. M. Johnson, M. M. Kennelly, D. Decesare, S. Morgan, and A. Sparrow, "Natural history of asymptomatic carotid plaque," *Arch Surg.*, vol. 120, pp. 1010–1012, 1985.

[23] B. Jones, *Statistics Toolbox for Use with MATLAB.* Natick, MA, USA: The MathWorks Inc., 1994.

[24] Y. M. Kadah, A. A. Farag, J. M. Zurada, A. M. Badawi, and A.-B. M. Youssef, "Classification algorithms for quantitative tissue characterization of diffuse liver disease from ultrasound images," *IEEE Trans. Med. Imag.*, vol. 15, pp. 466–478, Aug. 1996.

[25] M. Langsfeld, A. C. Gray-Weale, and R. J. Lusby, "The role of plaque morphology and diameter reduction in the development af new symptoms in asymptomatic carotid arteries," *J. Vasc. Surg.*, vol. 9, no. 4, pp. 548–557, 1989.

[26] G. L. Londrey, D. P. Spadone, K. J. Hodgson, D. E. Ramsey, L. D. Barkmeier, and D. S. Sumner, "Does Color-flow imaging improve the accuracy of duplex carotid evaluation?," *J. Vasc. Surg.*, vol. 13, no. 5, pp. 659–663, 1991.

[27] A. M. Mazzone, M. P. Urbani, E. Picano, M. Paterni, E. Borgatti, A. De Fabritiis, and L. Landini, "*In vivo* ultrasonic parametric imaging of carotid atherosclerotic plaque by videodensitometric technique," *Angiol.*, vol. 46, no. 8, pp. 663–672. 1995.

[28] M. L. Neale, J. L. Chambers, A. T. Kelly, S. Connard, M. A. Lawton, J. Roche, and M. Appleberg, "Reappraisal of duplex criteria to assess significant carotid stenosis with special reference to reports from the North American Symptomatic Carotid Endarterectomy Trial and the European Carotid Surgery Trial," *J. Vasc. Surg.*, vol. 20, no. 4, pp. 642–649, 1994.

[29] D. Nicholas, D. K. Nassiri, P. Garbutt, and C. R. Hill, "Tissue characterization from ultrasound B-scan data," *Ultrasound in Med., Biol.*, vol. 12, no. 2, pp. 135–143, 1986.

[30] "North American symptomatic carotid endarterectomy trial collaborators (NASCET): Beneficial effect of carotid endarterectomy in symptomatic patients with high-grade carotid stenosis," *New Eng. J. Med.*, vol. 325, no. 7, pp. 445–453, 1991.

[31] T. F. O'Donnell, L. Erdoes, W. C. Mackey, J. McCullough, A. Shepard, P. Heggerick, J. Isner, and A. D. Callow," "Correlation of B-mode ultrasound imaging and arteriography with pathologic findings at carotid endarterectomy," *Arch Surg.*, vol. 120, pp. 443–449, 1985.

[32] L. W. O'Holleran, M. M. Kennelly, M. McClurken, and J. M. Johnson, "Natural history of asymptomatic carotid plaque," *Amer. J. of Surg.*, vol. 154, pp. 659–662, 1987.

[33] P. C. Pedersen, "Ultrasound technique for arterial plaque characterization based on absolute backscatter measurements," *Ultrason. Imag.*, vol. 19, no. 1, pp. 46–47. 1997.

[34] E. Picano, L. Landini, A. Distante, M. Salvadori, F. Lattanzi, M. Masini, and A. L'Abbate, "Angle dependence of ultrasonic backscatter in arterial tissues: A study *in vitro*," *Circ.*, vol. 72, no. 3, pp. 572–576, 1985.

[35] W. H. Press, S. A. Teukolsky, W. T. Vetterling, and B. P. Flannery, *Numerical Recipes in C. The Art of Scientific Computing.* Cambridge, U.K.: Cambridge Univ. Press, 2nd ed., 1992, p. 703.

[36] U. Raeth, D. Schlaps, B. Limberg, I. Zuna, A. Lorenz, G. van Kaick, W. J. Lorenz, and B. Kommerell, "Diagnostic accuracy of computerized B-scan texture analysis and conventional ultrasonography in diffuse parenchymal and malignant liver disease," *J. Clin. Ultrasound*, vol. 13, pp. 87–99, 1985.

[37] L. M. Reilly, R. J. Lusby, L. Hughes, L. D. Ferrell, R. J. Stoney, and W. K., "Carotid plaque histology using real-time ultrasonography. Clinical and therapeutic implications," *Amer. J. Surg.*, vol. 146, pp. 188–193, 1983.

[38] A. V. Sterpetti, R. D. Schultz, R. J. Feldhaus, K. L. Davenport, M. Richardson, C. Farina, and W. J. Hunter, "Ultrasonographic features of carotid plaque and the risk of subsequent neurologic deficits," *Surg.*, vol. 104, no. 4, pp. 652–660, 1988.

[39] F. M. J. Valckx and J. M. Thijssen, "Texture classification of echographic images by means of the co-occurrence matrix," *Acoust. Imag.*, vol. 22, pp. 299–302, 1996.

[40] C.-M. Wu, Y.-C. Chen, and K.-S. Hsieh, "Texture features for classification of ultrasonic liver images," *IEEE Trans. Med. Imag.*, vol. 11, pp. 141–152, Apr. 1992.